JOURNAL OF EXPERIMENTAL AND THEORETICAL PHYSICS, 2024, Vol. 165, No. 4, pp. 489–496

ATOMS, MOLECULES, OPTICS

DIFFUSE X-RAY SCATTERING ON 1-DODECANOL FILM AT THE N-HEXANE-WATER INTERFACE

© 2024 A. M. Tikhonov[a,*], Yu. O. Volkov [b,c,**]

[a]Kapitza Institute for Physical Problems, Russian Academy of Sciences, 119334, Moscow, Russia

[b]National Research Center "Kurchatov Institute", 123182, Moscow, Russia

[c]Osipyan Institute of Solid State Physics, Russian Academy of Sciences, 142432, Chernogolovka, Moscow Region, Russia

*e-mail: tikhonov@kapitza.ras.ru

**e-mail: volkov.y@crys.ras.ru

Received October 27, 2023
Revised December 05, 2023
Accepted December 06, 2023

Abstract. Using a model-independent approach, experimental diffuse scattering data obtained with 15 keV synchrotron radiation were used to compare spectral characteristics of height-height correlation functions for pure n-hexane-water interface and with the presence of 1-dodecanol adsorption film. The observed scattering intensity in the case of pure interface is described by diffuse scattering on a structure with capillary-wave spectrum. In the presence of adsorption film, according to the analysis, the observed scattering intensity is mainly due to the contribution of grazing small-angle scattering on the near-surface micellar layer. In this case, the spectrum acquires a specific non-capillary-wave nature.

Keywords: *x-ray scattering, x-ray reflectivity, liquid-liquid interface, adsorption, thin films*

DOI: 10.31857/S004445102404e035

1. INTRODUCTION

In soluble adsorption films of long-chain saturated monoatomic alcohols (1-alkanols), for example, at the saturated hydrocarbon-water interface, a liquid-vapor phase transition is observed with increasing temperature, during which the adsorbate almost completely transfers into the bulk phase of the hydrocarbon solvent. The transition can have not only thermotropic but also barotropic or lyotropic nature [1,2]. Previously, in work [3], it was reported that thermotropic transitions in films of 1-dodecanol ($C_{12}OH$) and 1-tetracosanol ($C_{24}OH$) at planar interfacial boundaries of n-hexane-water and n-hexadecane-water, respectively, are characterized by relatively low transition enthalpy ΔH with corresponding values of approximately 0.05 mJ/m^2 and 0.07 mJ/m^2. In the same work, based on experimental data from film reflectometry using hard synchrotron radiation within a model approach, a structure with a thickness of two to three monolayers was proposed, and, moreover, the transition to complete wetting of the water subphase surface by the alkanol film was discussed. Recently, in work [4], using a model-independent approach [5], the parameters of layers $C_{12}OH$ and $C_{24}OH$ were refined. It is shown that in the low-temperature mesophase, the film consists of a soluble Gibbs monolayer 1 (Fig. 1), a transitional diffuse liquid layer 2 with a thickness of two to three monolayers (approximately 50 Å) and an extended (up to 200 Å wide) micelle layer 4. Quite unexpectedly, using the model-independent approach to reconstruct the electron concentration profile, the presence of a plane of least approach of the micellar layer to the interfacial boundary was established, which is located at a distance of about 100 Å from the n-hexane boundary or about 25 Å from the adsorption film (depleted layer 3). During the thermotropic transition to the high-temperature mesophase, there is a decrease in density and partial evaporation of the 1-alkanol adsorption film, which is also accompanied by depletion of the micellar layer until its complete

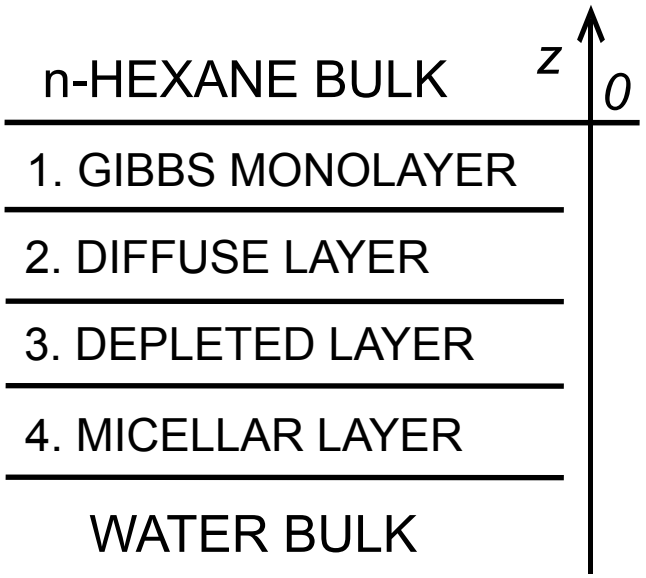

Fig. 1. Structure of the 1-dodecanol adsorption film according to model-free reconstruction [4]

disappearance. In this case, the Gibbs monolayer, unlike the thermotropic behavior of an insoluble Langmuir monolayer, partially dissolves in the oil phase.

Here we present new experimental data on grazing diffuse scattering at the n-hexane-water interface in the presence of an adsorption film $C_{12}OH$ which, in particular, independently confirms the presence of a near-surface micellar layer 4, predicted by model-free reconstruction [4].

2. EXPERIMENT

Samples of the planar n-hexane-water interface, oriented by gravity, were prepared and studied in a thermostated stainless steel cell with X-ray transparent polyethylene glycol terephthalate windows according to the method described in [6]. The interface with geometric surface dimensions of approximately 75 mm along and 150 mm across the X-ray beam was formed between the upper oil phase of about 50 ml and the aqueous phase of about 100 ml. Then, a two-stage thermostat with the experimental cell was mounted on the optical table of the X-ray spectrometer equipped with an active vibration isolation system. To prevent gas bubble formation at the interface, the sample was "annealed": first, the temperature of liquids in the cell was raised to approximately 330 K, then the sample was equilibrated at the set temperature for at least 12 hours.

As the oil phase, either n-hexane purified by multiple filtration in a chromatographic column C_6H_{14} (Aldrich-Sigma, boiling point $T_b \approx 342$ K and density at $T = 298$ K is approximately 0.65 g/cm^3), or solution $C_{12}OH$ in purified hydrocarbon with concentration $c \approx 45$ mMol/kg [7] was used. The monohydric alcohol 1-dodecanol purchased from AldrichSigma ($C_{12}H_{26}O$, purity >99%) was used in the experiment without additional purification. The total length of L_{trans}-dodecanol molecules is determined by the length of the carbon chain (approximately 1.27 Å per C-C), the sizes of the methyl-CH_3 (approximately 1.5Å) and hydroxyl-CH_2OH (about 2.4 Å) groups [8]. Thus, $L_{trans} \approx 18$ Å.

As the lower phase, either ultrapure deionized water (Barnstead, NanoPureUV, pH = 7, specific electrical resistance is about 18.2 MΩ/m·cm), or NaCl solution in it with a concentration of about 5 Mol/L was used. The temperature dependence for interfacial tension in the case of 1-dodecanol film at the n-hexane-water interface at the selected value c was previously published in [3]: it established the temperature value of the thermotropic transition in the film at $T_c \approx 310$.

The inset in Fig. 2 illustrates the kinematics of elastic surface X-ray scattering at the interface. The z axis is oriented along the surface normal in the direction opposite to the gravitational force. In the experiment in the yz plane, the grazing angle is $\alpha \ll 1$, the scattering angle is $\beta \ll 1$, and the azimuthal angle xy between the incident beam direction and the scattering direction is $\phi \approx 0$. In this coordinate system, the components of the scattering vector $q = k_{in} - k_{sc}$ (where k_{in}, k_{sc} are the wave vectors of incident and scattered beams in the direction of the point detector) have the following form: $q_x \approx k_0\phi$ and $q_y \approx k_0(\alpha^2 - \beta^2)/2$ in the interface plane xy ($k_0 = 2\pi/\lambda$), and along the normal $q_z \approx k_0(\alpha + \beta)$.

Information about the normal to the surface and lateral structure of n-hexane-water interfaces was obtained from measurements of the reflection coefficient R as a function q_z at $\alpha = \beta$ and the intensity of diffuse scattering I as a function of angle β at fixed $\alpha = \alpha$ using a monochromatic synchrotron radiation photon beam with a wavelength of $\lambda = 0.825 \pm 0.002$ Å and intensity of about 10^{10} photon/s at the X19C beamline of NSLS synchrotron [9].

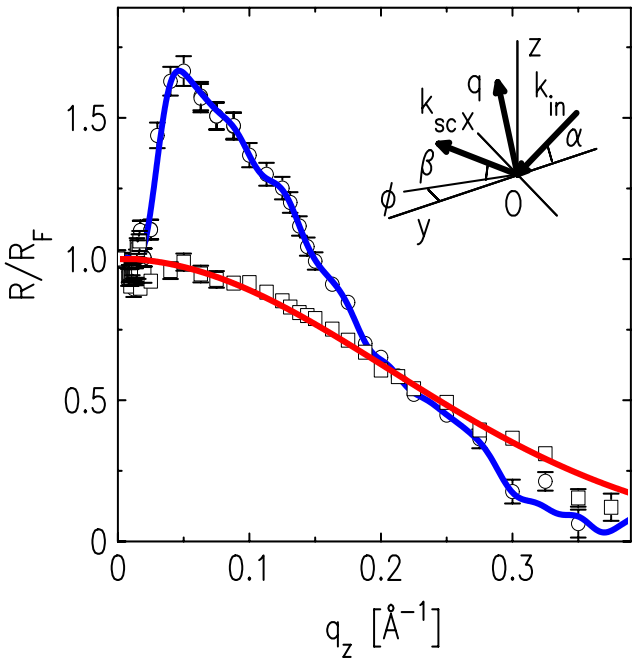

Fig 2. Dependence of the reflection coefficient, normalized to the Fresnel function, from the pure n-hexane-water interface (squares, $T \approx 297$) and adsorption film $C_{12}OH$ (circles, $T \approx 293$ K). The concentration of n-alkanol in n-hexane is 45 mmol/kg. Inset: scattering kinematics at a flat interface

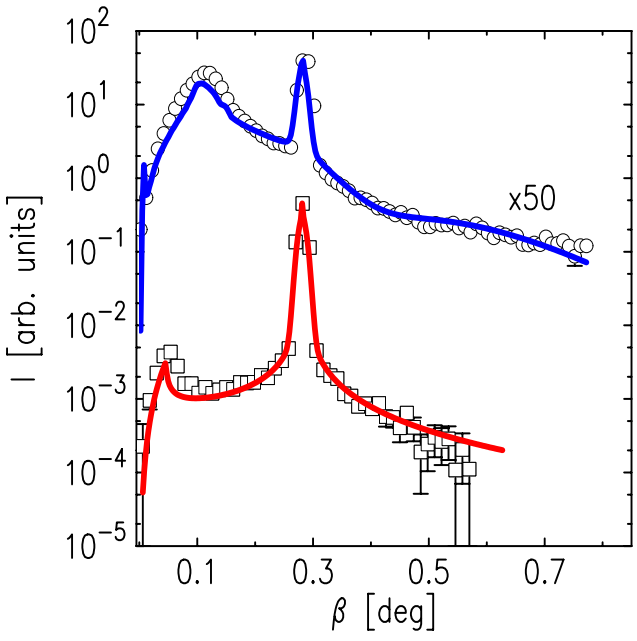

Fig. 4. Dependence of scattering intensity $I(\beta)$ at grazing angle $\alpha' \approx 0.29°$ from pure n-hexane-water interface (squares, $T \approx 297$ K) and in the presence of adsorption film $C_{12}OH$ (circles, $T \approx 293$ K). Blue line is calculation based on model-independent reconstruction of electron density profile, red line is calculation for capillary-wave structure

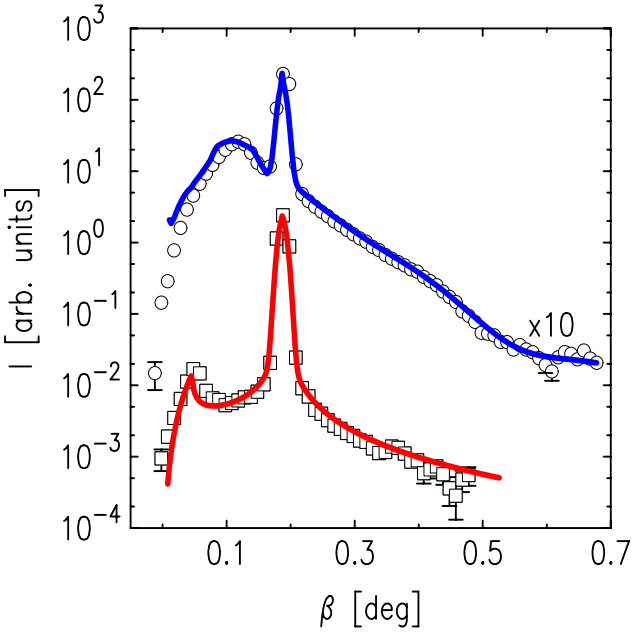

Fig. 3. Dependence of scattering intensity $I(\beta)$ at grazing angle $\alpha' \approx 0.19°$ from pure n-hexane-water interface (squares, $T \approx 297$ K) and in the presence of adsorption film $C_{12}OH$ (circles, $T \approx 293$ K). Blue line is calculation based on model-independent reconstruction of electron density profile, red line is calculation for capillary-wave structure

Previously, using these methods, research was conducted to study, for example, the structures of polymer coatings on flat surface of single-crystal silicon [10], organoclay layers on water surface [11] and phospholipid multilayers on silica hydrosol surface [12], as well as the dependence of octadecanamide adsorption film structure at toluene-water interface on pH level of aqueous subphase [13].

Fig. 2 shows the dependencies $R(q_z)$, normalized to the Fresnel function

$$R_F(q_z) = \frac{(q_z - [q_z^2 - q_c^2]^{1/2})^2}{(q_z + [q_z^2 - q_c^2]^{1/2})^2},$$

for the pure n-hexane-water interface (squares, $T \approx 297$ K and the interface with an adsorption film $C_{12}OH$ (circles, $T \approx 293$ K). At $q_z < q_c \approx 2k_0\alpha_c$ the incident beam undergoes total external reflection $R \approx 1$. The value of the total external reflection angle $\alpha_c = \lambda\sqrt{r_e\Delta\rho / \pi}$ (where $r_e = 2.814 \cdot 10^{-5}$ Å which is the classical electron radius) for n-hexane-water interfaces is determined by the difference $\Delta\rho = \rho_w - \rho_h$ in bulk electron concentrations in the hydrocarbon solvent $\rho_h \approx 0.23$ $e^-/Å^3$ and aqueous subphase. For pure water $\rho_w \approx 0.333$ $e^-/Å^3$, and for

salt solution it is about 0.38 $e^-/Å^3$. Thus, for the n-hexane-pure water interface with a film $C_{12}OH$ $\alpha_c \approx 7.9 \cdot 10^{-4}$ rad, ($q_c \approx 0.012$ $Å^{-1}$) and for the n-hexane solution interface NaCl $\alpha_c \approx 10^{-3}$ rad ($q_c \approx 0.015$ $Å^{-1}$).

Note that in the structural factor of the n-hexane-water interface $R(q_z) / R_F(q_z)$ with an adsorption film $C_{12}OH$ a peak is observed at $q_z' \approx 0.05$ $Å^{-1}$ which corresponds to a near-surface structure with a thickness of at least $2\pi / q_z' \approx 100$ Å. In the case of a pure n-hexane-NaCl solution interface, the structural factor has no apparent features.

When measuring R and I at small glancing angles α there are limitations related to the vertical size and divergence of the synchrotron radiation beam [14]. The reduction of natural beam divergence from approximately 10^{-4} rad to a value of about 10^{-5} rad was achieved using two input slits with a gap in the range of about 10 μm at a distance of approximately 600 mm, which ensures that only a flat section of the interfacial boundary is irradiated in the experiment, with an estimated width along the beam propagation direction of about 20 mm. The vertical angular resolution of the detector during $R(q_z)$ measurements is $\Delta\beta \approx 10^{-3}$ rad (slit with vertical gap 0.8 mm at a distance of approximately 680 mm from the sample center). When measuring the scattering intensity $I(\beta)$ the vertical size of the incident beam at the sample surface is approximately 0.05 mm, and the angular resolution of the point detector in the incidence plane is $\Delta\beta \approx 3 \cdot 10^{-4}$ rad. In all experiments, the angular resolution in the horizontal plane is $\Delta\phi \approx 10^{-2}$ rad. With these geometric dimensions of the incident beam (more than 5 μm in the vertical plane and about 2 mm in the horizontal), the averaging of values $R(q_z)$ and $I(\beta)$ in the experiment occurs over the illuminated area $S \le 0.3$ cm^2.

In Figs. 3 and 4, the dependencies of surface scattering intensity

$$I(\beta) = \frac{I_{sc}(\beta) - I_b(\beta)}{I_0}$$

at $\alpha' \approx 3.3 \cdot 10^{-3}$ rad (approximately 0.19°) and approximately $5 \cdot 10^{-3}$ rad (approximately 0.29°) respectively from the pure n-hexane-water interface (squares, $T \approx 297$ K) and in the presence of an adsorption film $C_{12}OH$ (circles, $T \approx 293$ K): I_{sc} – number of photons specularly reflected, diffusely scattered by the surface in the illuminated area at the center of the interfacial boundary of the sample and by the volume of the oil phase in the direction β. For independent determination of the contribution of photons scattered in the n-hexane volume $I_b(\beta)$ along the path to the boundary, the experimental cell with the sample was lowered along the axis z by approximately 0.2 mm so that the beam passed slightly above the phase interface. In this case, the registered background value increases to approximately $2I_b$, as the path length of the X-ray beam in the hydrocarbon solvent increases by approximately the same factor ($I_b(\beta) \sim 5 \cdot 10^{-4} I_s(\alpha')$). Finally, I_0 is a value proportional to the incident beam intensity, which was monitored in the experiment directly before the beam entered the cell using a second detector. On the scattering curves, the most intense peak corresponds to specular reflection $\beta = \alpha'$, and the peak in the diffuse background for the pure interface at $\beta \to 0$ corresponds to the angle of total external reflection $\alpha_c \approx 10^{-3}$ rad (approximately 0.05°) [15].

3. THEORY

Reflection $R(q_z)$ and scattering $I(\beta)$ from the interfacial boundary are described within the formalism of the distorted wave Born approximation [16]:

$$\frac{R(q_z)}{R_F(q_z)} = \left|\Phi(q_z)\right|^2 \tag{1}$$

and

$$I(q) \propto \left|\psi(\alpha)\psi(\beta)\right|^2 \left|\Phi(q)\right|^2 \bar{C}(\nu), \tag{2}$$

where $\psi(\theta)$ is the field amplitude of the wave with radiation polarization in the plane of the interfacial boundary, Φ is the structural factor of the interfacial boundary (Fourier transform of the derivative of the electron concentration distribution ρ along the axis z, averaged over the illuminated area S):

$$\Phi(q) = \frac{1}{\Delta\rho} \int_{-\infty}^{+\infty} \left\langle \frac{d\rho(z)}{dz} \right\rangle e^{iqz} dz, \tag{3}$$

and $\bar{C}$ is a one-dimensional function of the spectral distribution of roughness correlations of the relief $\zeta(x, y)$in the interface plane xOy [17]:

$$\bar{C}(\nu) = \int \left\langle \zeta(0)\zeta(u) \right\rangle e^{2i\pi u\nu} du, \tag{4}$$

where $\nu = | q_{xy} | /2\pi$ is the modulus of the wave vector projection onto the interface plane (spatial

frequency), and u is the modulus of the distance vector from point O in the interface plane.

In turn, the electron concentration profile for the adsorption film at the interfacial boundary (scheme in Fig. 1) can be defined by a parametric n-layer model based on the error function $erf(x)$:

$$\langle\rho(z)\rangle = \sum_{j=1}^{n}\frac{1}{2}(\rho_j - \rho_{j-1})erf\left(\frac{z-z_j}{\sigma\sqrt{2}}\right), \quad (5)$$

with a model parameter σ that sets the interface width between adjacent layers.

For liquid surfaces, the roughness spectrum $\bar{C}_{cap}$ and interlayer width σ are traditionally interpreted in the standard capillary wave theory [18]:

$$\bar{C}_{cap}(\nu) = \frac{k_BT}{4\pi^2\gamma(T)}\cdot\frac{1}{\nu^2 + \sqrt{(\rho_V g)/\gamma(T)}}, \quad (6)$$

where ρ_V is the bulk phase density, γ is the surface tension, k_B is the Boltzmann constant. Accordingly, the effective height of capillary roughness (capillary width)

$$\sigma_{cap}^2 = 2\pi\int_{1/L}^{1/\lambda}\bar{C}_{cap}(\nu)d\nu, \quad (7)$$

where L is the characteristic linear dimension of the surface. In the scattering experiment in the hard region of the spectrum

$$\sigma_{cap}^2 = \frac{k_BT}{2\pi\gamma(T)}\ln\left(\frac{Q_{max}}{Q_{min}}\right), \quad (8)$$

i.e., the observed width is determined by the short-wave limit in the capillary wave spectrum $Q_{max} = 2\pi/a$ ($a \approx 10$ Å on the order of intermolecular distance) and the angular resolution of the detector $Q_{min} = q_z^{max}\Delta\beta/2$ ($q_z^{max} \approx 0.4$ Å^{-1} is maximum value of q_z in the experiment) [19, 20].

Assuming that in the presence of an adsorption film (see Fig. 1) the roughness of the Gibbs monolayer and micellar layer are completely uncorrelated, the scattering intensity can be represented as the sum of components:

$$I(q) = I_{cap}(q) + \eta I_{mic}(q), \quad (9)$$

where non-capillary scattering on micelles $I_{mic}(q)$ is described similarly to expression (2), and η is the volume filling coefficient of the layer with micelles. In the case of spherical micelles with radius r, distributed in a micellar layer of thickness D, the structural factor of the layer can be represented as the product of the form factor of a single micelle [21] and the Fourier transform of the micelle distribution by depth:

$$\Phi(q,r) = \frac{\sin(qr) - qr\cos(qr)}{(qr)^3}\int\frac{\rho(z)}{\rho_h}e^{iqz}dz. \quad (10)$$

In turn, for the statistical characterization of the non-capillary roughness component, the K – correlation model was used [22]

$$\bar{C}_{KC}(\nu) = \frac{A}{\left[1 + B^2\nu^2\right]^{(h+1)/2}}, \quad (11)$$

where A is the normalization factor in the low-frequency limit of the spectrum, determining the effective value σ; B is the critical correlation radius and h is the fractal parameter.

4. EXPERIMENTAL RESULTS AND DISCUSSION

The thermodynamics of the Gibbs adsorption film at the liquid-liquid interface is described by parameters p – pressure, T – temperature and c – alcohol concentration in the bulk of the hydrocarbon solvent [23–25]. In the case of thermotropic transition (p = 1 atm and c=const) in the adsorption film of 1-alkanol at the hydrocarbon-water interface, a feature (break) is observed on the temperature dependence of interfacial tension $\gamma(T)$ at T_c, which can be associated with enthalpy change

$$\Delta H = -T_c\Delta(\partial\gamma/\partial T)_{p,c}.$$

According to experimental observations, thermotropic liquid-vapor phase transitions are observed in layers of fluorinated 1-alkanols [26,27], while solid-gas transitions occur in fluoroalkanol films [28]. Similar phenomena have also been discovered in the adsorption film consisting of a mixture of alkanol and fluoroalkanol [29].

The value ΔH is practically independent of the bulk concentration c. For example, in [30] this is demonstrated for the lyotropic transition at the n-hexane-water interface in the 1-eicosanol film ($C_{20}OH$). Fig. 5 illustrates the dependence of ΔH on the m ratio of the number of carbon atoms in alkanol (labels at points) to the number of carbon atoms in the solvent molecule: points and circles – data for n-hexane-water interface, squares – for n-hexadecane-water interface. It is quite unexpected that for fluorinated 1-alkanol films $FC_{10}OH$ and $FC_{12}OH$, which sublimate upon heating at the

n-hexane-water interface, the values of ΔH are very close to the enthalpy change of normal alcohols $C_{24}OH$ and $C_{30}OH$ at the n-hexadecane-water interface respectively. A more detailed discussion of Fig. 5 is available in [3].

Note that the change in surface state at T_c can be either sharp or prolonged in temperature transition with the formation of spatially inhomogeneous structures at the boundary [31]. For example, in a fluorinated alcohol film $FC_{10}OH$ $\Delta H \approx 0.15$ mJ/m², the observed transition width $\Delta T_c > 10$ K [32], while for the film $C_{22}OH$ with relatively large $\Delta H \approx 0.7$ mJ/m² range $\Delta T_c < 0.01$ K [27]. The process of fragmentation and mixing of low-temperature and high-temperature phases, which have different surface polarization, is caused by the long-range nature of the electric field decay E from the linear boundary between surface phase domains ($E \propto 1/l$, where l is distance) and significantly reduces the surface energy [33]. However, short-range van der Waals interactions, determining the energy of linear tension of the domain boundary, limit the growth of one-dimensional boundary length. Formally, this imposes a prohibition on first-order transition in the electric double layer at the liquid-liquid interface [34], instead of which an infinite chain of phase transitions (critical crossover) can be realized [35,36].

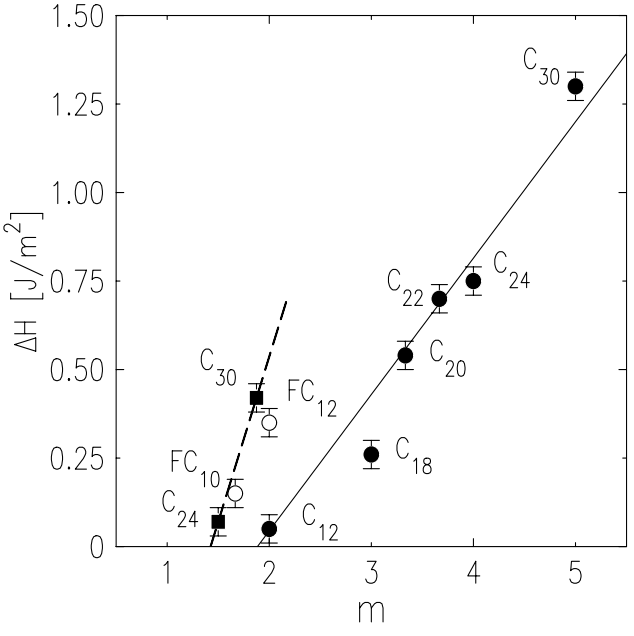

Fig. 5. Enthalpy change ΔH during phase transition at the hydrocarbon-water interface in the adsorption film of long-chain alcohol as a function of the ratio of carbon atoms in alkanol (labels at points) to the number of carbon atoms in the solvent molecule m. Points and circles – data for n-hexane-water interface, squares – n-hexadecane-water interface. Lines are drawn for better visualization of results

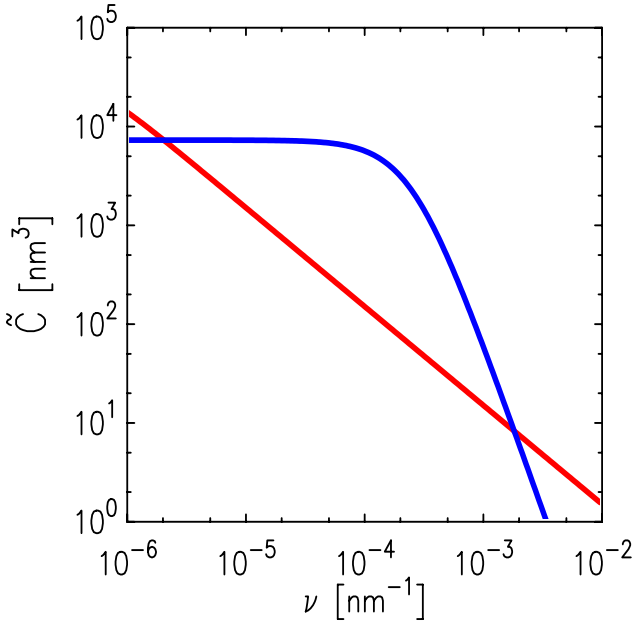

Fig. 6. Components of roughness correlation function spectra $\bar{C}(\nu)$ for capillary-wave structure at the interface (red line) and for micellar layer (blue line)

Due to the small difference in surface energy between low-temperature and high-temperature film phases $C_{12}OH$ ($\Delta H \approx 0.05$ mJ/m²), a sufficiently wide temperature range ΔT_c should be expected, in which a spatially inhomogeneous structure appears in the adsorption film. Perhaps for this reason, in the high-temperature phase of the $C_{12}OH$ film the gas phase is not realized in pure form up to the boiling point of n-hexane at $T \approx 342$ K, and a monolayer structure is observed with hydrocarbon tail packing density noticeably lower $\rho_{C12} \approx 0.7\rho_w$ [4] than the electronic concentration in high-molecular-weight alkane liquid, which corresponds to $0.8\rho_w$–$0.9\rho_w$ a homogeneous disordered monolayer [8,27].

In the case of a clean n-hexane/NaCl solution interface, the calculated curves (red lines in Figs. 2, 3, and 4) for both the reflection coefficient [16]

$$\frac{R(q_z)}{R_F(q_z)} = e^{-q_z q_z^t \sigma_{cap}^2}, \qquad (12)$$

where

$$q_z^t \approx k_0\left(\sqrt{\alpha^2 - \alpha_c^2} + \sqrt{\beta^2 - \alpha_c^2}\right),$$

and the scattering curve $I_{cap}(\beta)$ demonstrate good agreement between the capillary wave model with

one fitting parameter σ_{cap} and experiment. The corresponding model spectrum $\bar{C}_{cap}$ at $\sigma_{cap} \approx 4$ Å is shown by the red line in Fig. 6. The value of the fitting parameter approximately coincides with the capillary width (3.5 ± 0.2) Å established from reflectometry data of the n-hexane-water interface [28]. Note that σ_{cap} is twice as smaller than the transition layer width (about 10 Å) on the surface of concentrated aqueous metal chloride solution reported in [37].

In the case of the 1-dodecanol adsorption film, the experimental diffuse scattering curves, besides the capillary component, show dominant scattering from the micellar layer. The calculated curves $I(\beta)$ from the adsorption film are shown by blue lines in Figs. 3 and 4; the model spectrum of the non-capillary component $\bar{C}_{KC}(\nu)$ is represented by the blue line in Fig. 6. The blue line in Fig. 2 corresponds to the film structural factor established during model-free reconstruction. The estimated filling coefficient of the micellar layer was $\eta = 0.11$, $B = 4.1$ μm, $h = 3.6$ with micelle radius $r \sim 18$ Å (which agrees with the estimate of the integral density of the micellar layer according to refined data in [4]). Note that for a partially filled layer ($\eta < 1$) the critical radius B corresponds to the characteristic linear size of scattering micelle clusters in the interface plane; however, the absence of diffraction peaks on the scattering curves in the region $\beta > \alpha'$ indicates their disordered distribution in the layer. In the roughness region corresponding to the experimental scattering angle interval ($\nu = 10^{-6} \ldots 10^{-3}$ nm^{-1}), the non-capillary component contribution dominates, while in the high-frequency region ($\nu > 10^{-3}$ nm, $\beta > 0.7^\circ$) the scattering is determined by capillary waves directly at the interface. The roughness estimate for the micellar layer according to (7) gives $\sigma \approx 19$ Å (parameter $A \approx 7.3 \cdot 10^3$ nm^3). More precise determination of the micellar layer structure requires measurement of two-dimensional diffuse scattering maps.

Thus, the observed scattering intensity $I(\beta)$ in the case of a pure interface is described by non-specular scattering on a structure with a capillary-wave roughness spectrum. In the presence of an adsorption film, the observed scattering intensity, according to the conducted analysis, is due to the contribution of grazing small-angle scattering on the near-surface micellar layer. The presence of such a layer in the interface structure was previously reported based on the results of model-free reconstruction of the electron density profile from reflectometry data of the interface [4]. The calculated roughness spectrum of the micellar layer also indicates spatial inhomogeneity in the distribution of micelles (clustering) in the interface plane. Thus, in the presence of an adsorption film and 1-dodecanol micelles, the spectrum of the height correlation function at the interface has a fundamentally non-capillary-wave nature.

FUNDING

The work was carried out within the framework of State Tasks of IPP RAS and NRC "Kurchatov Institute". The theoretical part of the work (Sections 3 and 4) was supported by a grant from the Russian Science Foundation (project No. 23-1200200).

REFERENCES

1. M. Lin, J. L. Ferpo, P. Mansaura, and J. F. Baret, J. Chem. Phys. 71, 2202 (1979).
2. Y. Hayami, A. Uemura, M. Ikeda, M. Aratono, and K. Motomura, J. Colloid Interface Sci. 172, 142 (1995).
3. A. M. Tikhonov and M. L. Schlossman, J. Phys.: Condens. Matter 19, 375101 (2007).
4. A. M. Tikhonov and Yu. O. Volkov, Surface. X-Ray, Synchrotron and Neutron Research, in press (2024).
5. I. V. Kozhevnikov, Nucl. Instr. Meth. Phys. Res. A 498, 482 (2003).
6. A. M. Tikhonov, V. E. Asadchikov, Yu. O. Volkov, A. D. Nuzhdin, B. S. Roshchin, PTE No. 1, 146 (2021).
7. A. Goebel and K. Lunkenheimer, Langmuir 13, 369 (1997).
8. D. M. Small, The Physical Chemistry of Lipids, Plenum Press, New York (1986).
9. M. L. Schlossman, D. Synal, Y. Guan, M. Meron, G. Shea-McCarthy, Z. Huang, A. Acero, S. M. Williams, S. A. Rice, and P. J. Viccaro, Rev. Sci. Instrum. 68, 4372 (1997).
10. L. Hanley, Y. Choi, E. R. Fuoco, F. A. Akin, M. B. J. Wijesundara, M. Li, A. M. Tikhonov, and M. L. Schlossman, Nucl. Instrum. Methods Phys. Res. B 203, 116 (2003).
11. J. Koo, S. Park, S. Satija, A. M. Tikhonov, J. C. Sokolov, M. H. Rafailovich, and T. Koga, J. Colloid and Interface Science 318, 103 (2008).
12. A. M. Tikhonov, JETP Letters 92, 394 (2010).
13. A. M. Tikhonov, Yu. O. Volkov, JETP 156, 440 (2019).

14. A. M. Tikhonov, JETP Letters 105, 737 (2017).

15. Y. Yoneda, Phys. Rev. 131, 2010 (1963).

16. S. K. Sinha, E. B. Sirota, S. Garoff, and H. B. Stanley, Phys. Rev. B 38, 2297 (1988).

17. D. J. Whitehouse, Surfaces and their Measurements, Hermes Penton, London (2002).

18. F. P. Buff, R. A. Lovett, and F. H. Stillinger, Phys. Rev. Lett. 15, 621 (1965).

19. A. Braslau, M. Deutsch, P. S. Pershan, A. H. Weiss, and J. Als-Nielsen, J. Bohr, Phys. Rev. Lett. 54, 114 (1985).

20. D. K. Schwartz, M. L. Schlossman, E. H. Kawamoto, G. J. Kellogg, P. S. Pershan, and B. M. Ocko, Phys. Rev. A 41, 5687 (1990).

21. J. S. Pedersen, Adv. Colloid and Interface Sci. 70, 171 (1997).

22. E. L. Church and P. Z. Takasz, Proc. SPIE 1530, 71 (1991).

23. J. W. Gibbs, Collected Works, Vol. 1, Dover, New York (1961), p. 219.

24. J. J. Jasper and B. L. Houseman, J. Phys. Chem. 67, 1548 (1963).

25. K. Motomura, J. Colloid Interface Sci. 64, 348 (1978).

26. N. Matubayasi, K. Motomura, M. Aratono, and R. Matuura, Bull. Chem. Soc. Jpn. 51, 2800 (1978).

27. A. M. Tikhonov, S. V. Pingali, and M. L. Schlossman, J. Chem. Phys. 120, 11822 (2004).

28. M. L. Schlossman, M. Li, D. M. Mitrinovic, and A. M. Tikhonov, High Performance Polymers 12, 551 (2000).

29. P. S. Venkatesh, T. Takiue, G. Guangming, A. M. Tikhonov, N Ikeda, M. Aratono, and M. L. Schlossman, J. Dispersion Science and Technology 27, 715 (2006).

30. T. Takiue, T. Matsuo, N. Ikeda, K. Motomura, and M. Aratono, J. Phys. Chem. B 102, 4906 (1998).

31. S. Uredat and G. Findenegg, Langmuir 15, 1108 (1999).

32. A. M. Tikhonov, M. Li, and M. L. Schlossman, J. Phys. Chem. B 105, 8065 (2001).

33. V. I. Marchenko, JETP Letters 33, 381 (1981).

34. V. I. Marchenko, JETP 81, 1142 (1981).

35. V. I. Marchenko, JETP 90, 2241 (1986).

36. A. M. Tikhonov, JETP 137, 1209 (2010).

37. E. Sloutskin, J. Baumert, B. M. Ocko, I. Kuzmenko, A. Checco, L. Tamam, E. Ofer, T. Gog, and M. Deutsch, J. Chem. Phys. 126, 054704 (2007).